Communication Analysis of tRNA-derived Fragment Uptake and Signalling in Neurons

Kurt J.A. Pumares*
Walton Institute
South East Technological University
Waterford, Republic of Ireland
kurt.pumares@waltoninstitute.ie
*Corresponding author

Daniel P. Martins
School of Comp. Science & Electronic Engg.
University of Essex
Colchester, UK
daniel.martins@essex.ac.uk

Steven Fagan
Dept. of Physiology & Medical Physics
Royal College of Surgeons in Ireland
Dublin, Republic of Ireland
steven.fagan@gmail.com

Rachel Stewart
Dept. of Physiology & Medical Physics
Royal College of Surgeons in Ireland
Dublin, Republic of Ireland
rachelstewart@rcsi.ie

Jochen H.M. Prehn
Dept. of Physiology & Medical Physics
Royal College of Surgeons in Ireland
Dublin, Republic of Ireland
jprehn@rcsi.ie

Deirdre Kilbane
Walton Institute
South East Technological University
Waterford, Republic of Ireland
deirdre.kilbane@waltoninstitute.ie

***Abstract*—Transfer RNAs (tRNAs) are a family of non-coding ribonucleic acids (RNAs) that are involved in protein translation. Cleavage of tRNA through stress-induced ribonucleases results in the production of short tRNA-derived small RNAs (tsRNAs), such as tRNA-derived fragments (tRFs). Recent studies have identified three tRFs–5'AlaTGC, 5'GluCTC, and 5'GlyGCC–to be released from neurons and significantly elevated in epilepsy patients. Extracellular 5'tRFs are taken up by neurons and act in paracrine to inhibit protein translation. We hereby explored a molecular communications (MC) approach to investigate biological effects of tRFs in neurons. Temporal dynamics and biophysical interactions of tRFs across the neuronal microdomain were expressed mathematically, and system communications performances were evaluated. The devised MC tool may aid in the interpretation of tRFs and their uptake and activities in neurons relevant to their potential as seizure biomarkers and neurotherapeutics.**

***Index Terms*—biological modeling, molecular communications, path loss, epilepsy, transferRNA, neurons, transfection**

I. Introduction

Epilepsy is a neurological disorder whereby a person has two or more unprovoked seizures which occur over 24 hours apart. Epileptic seizures occur due to an imbalance between neuronal excitation and inhibition pathways [1], [2]. Diagnosis of seizure type is determined by a neurologist using electroencephalogram (EEG) and magnetic resonance imaging (MRI) technology, however there are currently very limited seizure prediction tools [3].

In recent years, researchers have explored small blood-transported molecules, such as non-coding ribonucleic acids (RNAs), as potential biomarker candidates for the prediction of seizures [4]. An example of functional noncoding RNAs are transfer RNAs (tRNAs) which are involved during protein synthesis by delivering amino acids to ribosomes [5]. Advances in RNA sequencing have identified fragments of tRNAs, termed short tRNA-derived small RNAs (tsRNAs), in protein translation inhibition and gene expression regulation, where tsRNAs particularly found in extracellular vesicles (EVs) take part in intercellular communication and act as potential biomarkers in human diseases [6]. Circulating EVs found in the bloodstream, as well as in plasma and serum, can deliver signalling molecules for uptake in cells to mediate cell-to-cell communications. tRNA-derived fragments (tRFs) are a group of tsRNAs that are generated from tRNA precursors (pre-tRNAs) or mature tRNAs by the activity of the ribonuclease Dicer [7]. Interestingly, members of this group were identified as novel biomarkers of seizure imminence in patients with temporal lobe epilepsy. Specifically, the three 5'tRFs 5'AlaTGC, 5'GluCTC, and 5'GlyGCC were found to be released from neurons during hyperexcitation and accumulated in plasma before seizure occurrence [8], [9]. Hence, exploring the mechanisms of transport and action of tRF is a promising research direction for the development of 5'tRFs as novel sensors of seizure imminence or novel neurotherapeutics.

Molecular communications (MC) has been applied in the modeling of molecular and drug delivery systems [10]–[13], and we here adapted this approach to characterise the delivery and uptake of tRFs into a neuronal cell, with EV-associated tRFs playing a key role in cellular communications. tRFs are secreted from neurons and transported in the brain by being loaded into EVs, specifically exosomes. To signal in paracrine, 5'tRFs then need to bind to the neuronal membrane before being internalized, and are subsequently used by the neurons to finetune gene expression and protein translation [14]. Here, we developed an MC model for the delivery of 5'tRFs between a molecular source and a receiver neuron. Specifically, we focus our analysis on the molecular dynamics to evaluate the overall communications performance of the tRF delivery system in terms of throughput and molecular processing-induced loss.

This study was funded by the European Union's EU-FET Open H2020 PRIME Project under Grant Agreement No. 964712, Science Foundation Ireland (SFI) under Grant Numbers 16/RC/3948 and 21/RC/10294_P2, European Regional Development Fund, and FutureNeuro industry partners.

II. System Model

We characterise the delivery system for 5'tRFs–5'AlaTGC, 5'GluCTC and 5'GlyGCC–in neurons using the MC paradigm in four stages: molecular transport, surface binding, internalization, and nuclear translocation, which are all fundamental to the regulation of gene expression and protein translation by 5'tRFs in the receiving neuron (molecular receiver). Fig. 1a describes the biochemical components of the neuronal microdomain investigated in this paper. First, 5'tRF-loaded exosomes (information signal) are emitted from a point source (information source) in the extracellular matrix (ECM) (molecular channel). These particles move towards the neuronal membrane and bind to surface receptors (information receptors). Afterwards, they are internalized and released into the cytosol (demodulator) from their encapsulating exosomes, before allowing their translocation to the nucleus (information destination) for gene expression and protein translation regulation, thus completing the paracrine signalling process. Fig. 1b illustrates the described cellular components and their processes as MC modules. We also abstracted our MC model into extra- and intra-cellular components, with further intracellular partitions representing the compartments for bound, internalized, and translocated information signals. We then considered these MC modules from a biophysical perspective and investigated their individual functions and interactions to design a characterisation of paracrine, source-to-neuron 5'tRF signalling and its impact on gene expression, protein synthesis inhibition, and seizure suppression.

A. Information Throughput Model

Our MC model is described as follows: an external information source emits the information signals into the molecular channel before being transported to the molecular receiver. These information signals will then bind to the information receptors, get internalized for signal demodulation, and finally arrive at the information destination. This molecular transport process is characterised by the movement of information signal concentrations (information symbols) across all MC modules. Inspired by [12], we then define information throughput (bioavailability) as a delay differential equation (DDE) which represents the supply of information signals in the molecular channel:

$$\frac{d[\mathrm{tRF}]_e(t)}{dt} = k_e - \alpha[\mathrm{tRF}]_e(t)(N - [\mathrm{tRF}]_b(t-\tau)), \quad (1)$$

where $[\mathrm{tRF}]_e$ denotes the information signal concentration in the molecular channel, k_e the fixed release rate of information symbols supplied into the molecular channel by the information source, α the binding rate of information symbols to the information receptor, τ the time delay in seconds accounting for the activation delay of the chemical rate equations, and N the surface capacity constant of information symbols. For the purposes of this study, the above kinetic equation assumes information symbols in the molecular channel are spatially averaged and diffusion and propagation properties ignored. Further assumptions were also established to neglect volume fraction and channel noise, both of which also dictate molecular propagation and anisotropic exosomal diffusion [15].

We then represent the intracellular delivery of information signals from the information receptors on the cell surface to the information destination in the nucleus by also using the MC paradigm. In biology, the uptake of tRF-loaded exosomes following their binding to the membrane is explained by the juxtacrine signalling, fusion, and endocytosis steps which describe transduction through intracellular signalling pathways, cellular membrane binding, and uptake and release from transport vesicles into the cytosol, all before translocation to the nucleus [14]. From an MC perspective, a fraction of the information throughput is received (binding) and demodulated (uptake) prior to arriving at the destination (translocation). The above fractions are then also expressed using DDEs as:

$$\frac{d[\mathrm{tRF}]_b(t)}{dt} = \alpha[\mathrm{tRF}]_e(t-\tau)(N - [\mathrm{tRF}]_b(t)) - k_c[\mathrm{tRF}]_b(t), \quad (2)$$

$$\frac{d[\mathrm{tRF}]_c(t)}{dt} = k_c[\mathrm{tRF}]_b(t-\tau) - k_n[\mathrm{tRF}]_c(t), \quad (3)$$

$$\frac{d[\mathrm{tRF}]_n(t)}{dt} = k_n[\mathrm{tRF}]_c(t-\tau) - k_t[\mathrm{tRF}]_n(t), \quad (4)$$

where $[\mathrm{tRF}]_b$, $[\mathrm{tRF}]_c$, and $[\mathrm{tRF}]_n$ denotes the information throughput fraction for binding, uptake, and translocation, respectively. The parameters k_c represents the internalization

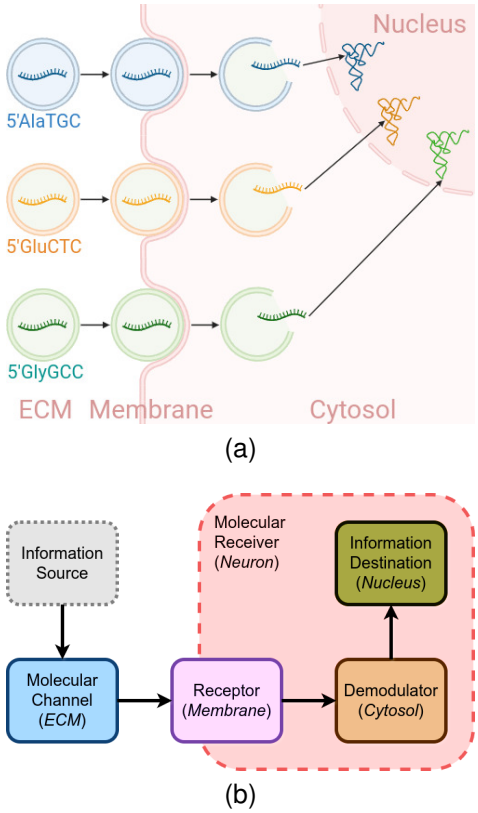

Fig. 1. Schematic diagram of tRF transfection process showing the (a) neuronal microdomain components and the (b) MC abstraction of paracrine 5'tRF signalling in neurons.

rate of information signals into the demodulator, k_n the translocation rate of information signals into the information destination, and k_t the translation/degradation rate of information signals in the information destination.

B. Molecular Processing-Induced Loss Model

As introduced in Section II-A, the information throughput is fractionated as it is processed by the neuron. Therefore, we also modelled this molecular processing-induced loss as a performance metric to observe the temporal dynamics and effects on tRF uptake in our MC model. Here, we assume a continuous release of molecules from the information source into the molecular channel with fixed rates as described in (1), influencing the molecular dynamics of the downstream MC modules described in (2)-(4) to have a sigmoid-like growth, which resembles the behaviour found in natural cells [16]. We also explored the propagation of molecules along a one-dimensional MC channel environment measured by distance [17] and the tortuosity of the media travelled by the molecules across MC modules [12], [18]. We then utilised a modified complementary error function as used in a similar approach [19] for the transmission rate function of tRFs with respect to an arbitrary normalised distance d from a source point x_s to an end point x_e and the normalised tortuosity λ as

$$T(d, \lambda) = (1 - \lambda) \cdot \mathrm{erfc}(4d - 2) \tag{5}$$

with $d = x_e - x_s$ such that $0 \leq x_s < x_e \leq 1$ as defined similarly for the path loss computation in [20] and $0 \leq \lambda \leq 1$ where $\lambda = 0$ represents the minimum tortuosity (free space movement) of the media between x_s and x_e while $\lambda = 1$ the maximum (impermeable). Based on the definition of path loss in [20], we use (1)-(5) to compute the general molecular processing-induced loss as follows:

$$P_{loss}(d, \lambda, C_{Tx}, C_{Rx}) = 10log_{10}\left(\frac{1}{T(d, \lambda)} \cdot \frac{C_{Tx}}{C_{Rx}}\right), \tag{6}$$

where C_{Tx} and C_{Rx} are the transmitted and received molecular concentrations in different MC modules, respectively. For example, we obtain the specific molecular processing-induced losses between compartments by considering $C_{Tx} = [tRF]_e$ and $C_{Rx} = [tRF]_b$ for the binding loss; $C_{Tx} = [tRF]_e$ and $C_{Rx} = [tRF]_c$ for the uptake loss; and $C_{Tx} = [tRF]_c$ and $C_{Rx} = [tRF]_n$ for the translocation loss.

III. Analysis Results

To observe the temporal dynamics of our proposed MC model, we conducted numerical simulations by solving the system in (1)-(4) using values for the release rate k_e, uptake rate k_c, translocation rate k_n, translation rate k_t, membrane binding rate α, and membrane binding constant N for 5'AlaTGC, 5'GluCTC, and 5'GlyGCC as listed in Table I. These parameters were fitted using data taken from a protein translation assay which was performed to quantify neuronal biological activity when neurons were exposed to specific tRFs, as provided in the supplementary material in https://dx.doi.org/10.21227/sdx0-z447. Mean fluorescence intensity (MFI) measured in arbitrary units is proportional to concentrations of fluorescently labelled 5'tRFs, and therefore can be used to quantify their levels for the evaluation of our information throughput results [21]. This proportionality facilitates a useful comparison between different fluorescence spectra, while higher concentrations lead to modifications in the fluorescence spectrum shape, as the fluorescence at shorter wavelengths is absorbed by other molecules. Noise and interference sources were ignored in order to conveniently validate our simulations with the experimental results, which could be explored in future works as Additive White Gaussian Noise (AWGN) [22], [23]. We set the initial tRF concentrations to 0 and assumed fixed release and degradation rates. Taking the molecular binding rate of the surface receptors into account, our temporal evaluations feature lower intracellular tRF concentrations in comparison to the extracellular space.

TABLE I
MC System Parameter Values

Parameter	5'AlaTGC	5'GluCTC	5'GlyGCC
k_e	0.1 s^{-1}	0.07 s^{-1}	0.11 s^{-1}
α	0.00001 s^{-1}	0.00001 s^{-1}	0.00001 s^{-1}
N	200	200	200
k_c	0.005 s^{-1}	0.006 s^{-1}	0.005 s^{-1}
k_n	0.0022 s^{-1}	0.003 s^{-1}	0.0023 s^{-1}
k_t	0.0027 s^{-1}	0.0035 s^{-1}	0.0038 s^{-1}

A. Information Throughput Analysis

The time curves obtained from evaluating the governing equations in (1)-(4) using the above parameter values are shown in Fig. 2a. The plots representing the availability of tRFs concentrations in four different locations follow our MC model topology: outside the cell (circle marker), bound to the cell membrane (cross marker), internalized in the cytosol (square marker), and translocated into the nucleus (triangle marker). We also observed that tRF levels follow a logistic growth and approach their upper limits after $t = 3600s$ ($t = 1h$), demonstrating the carrying capacity of each MC module. Therefore, the collective modular dynamics of our proposed delivery system characterises the entire tRF delivery process in neurons, in which similar molecular concentration behaviours were observed in [16]. Furthermore, the observed high MFI levels (i.e., molecular throughput) can be associated with an enhanced impact on the inhibition of seizure-related protein synthesis, confirming results obtained in another study [24]. Hence, our results validated our MC model and served as the basis for our next analyses, which includes the selection of our tRF of interest (5'AlaTGC having the highest concentration in the nucleus).

Next, we varied three parameter values (surface binding rate α, surface capacity constant N, and time delay τ) to explore their effects on the tRF concentration dynamics across the MC modules, and consequently, the overall communications performance of the tRF delivery system in neurons. Fig. 2b shows that when α is increased, lower 5'AlaTGC MFI levels in the ECM are obtained since stronger cell surface adhesion

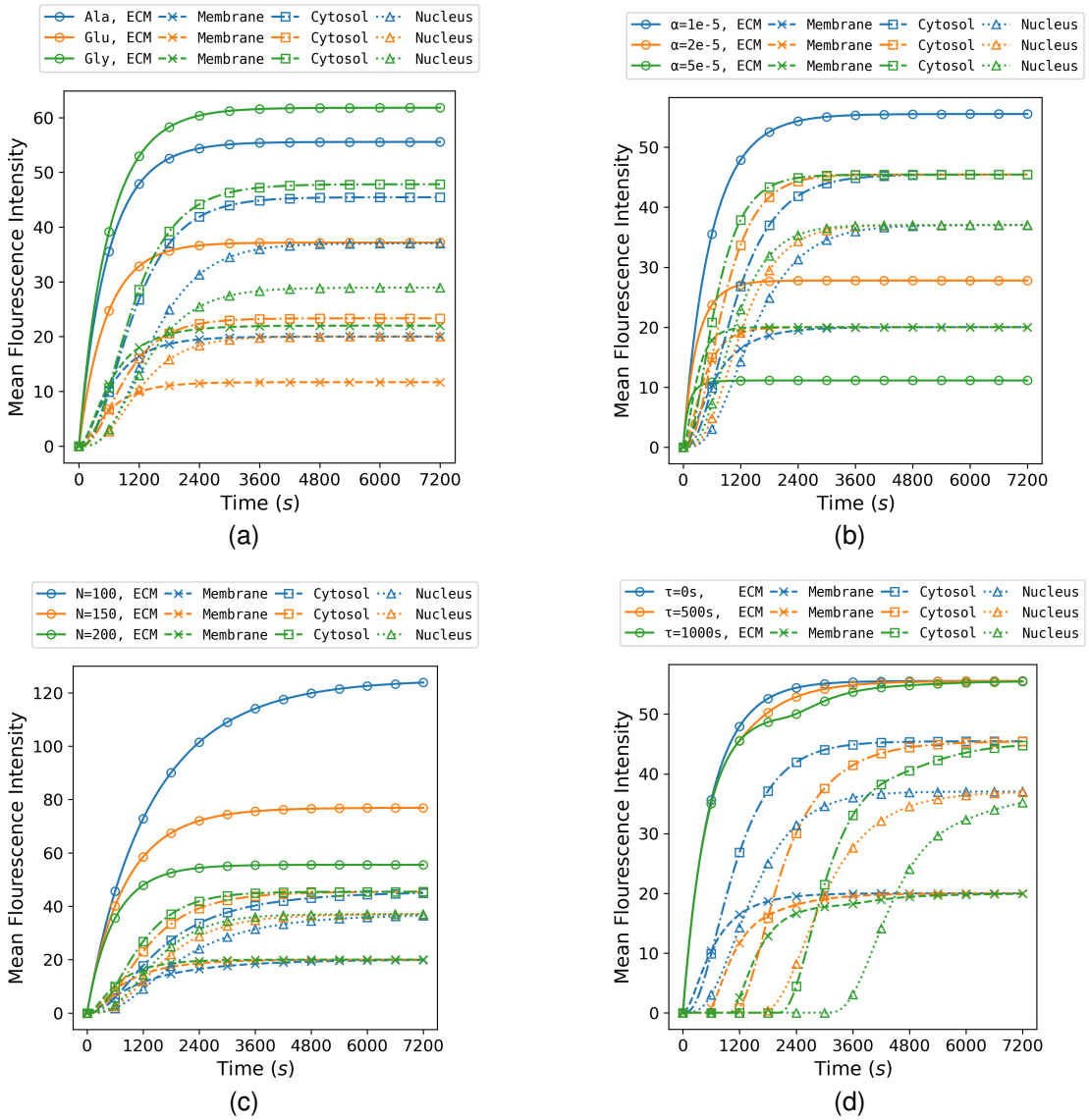

Fig. 2. tRF concentration profiles across MC modules showing the (a) temporal evaluation and 5'AlaTGC response to varying (b) surface binding rate α, (c) surface capacity constant N, and (d) time delay τ.

results in more molecules bound to the cell membrane, and therefore, fewer molecules present in the ECM. Furthermore, the 5'AlaTGC MFI levels under higher α values in the membrane, cytosol, and the nucleus reached their upper limits faster due to an increased internalization of molecules by the cell. Meanwhile, Fig. 2c shows that lowered N values would result in much higher 5'AlaTGC MFI levels in the ECM since fewer molecules could bind to the cell membrane. Interestingly, changing the parameter values for α or N has no effect on the respective carrying capacities of the membrane, cytosol, and the nucleus, but only on the time required to reach such levels. Lastly, we considered a time delay τ in our information throughput analysis. Fig. 2d shows that the time required to reach the maximum information throughput for the ECM and the cell membrane was barely delayed, in comparison with those for the cytosol and the nucleus. This shows that the demodulation and internalization processes are critical points for tRF transfection affected by molecular delays.

B. Molecular Processing-Induced Loss Analysis

We used (5) and (6) together with our simulation setup to compute the path loss induced by molecular processing in each MC module. Please note that in this analysis, we did not evaluate other common losses found in MC models such as propagation losses. Our focus was on measuring the amount of molecular processing-induced loss that are able to reach the receiving neuron. First, we plot the computed losses versus the normalised distance between a point source to the destination. Next, we evaluated these losses under low, mid, and high values for normalised channel tortuosity λ, surface binding rate α, surface capacity constant N, and time delay

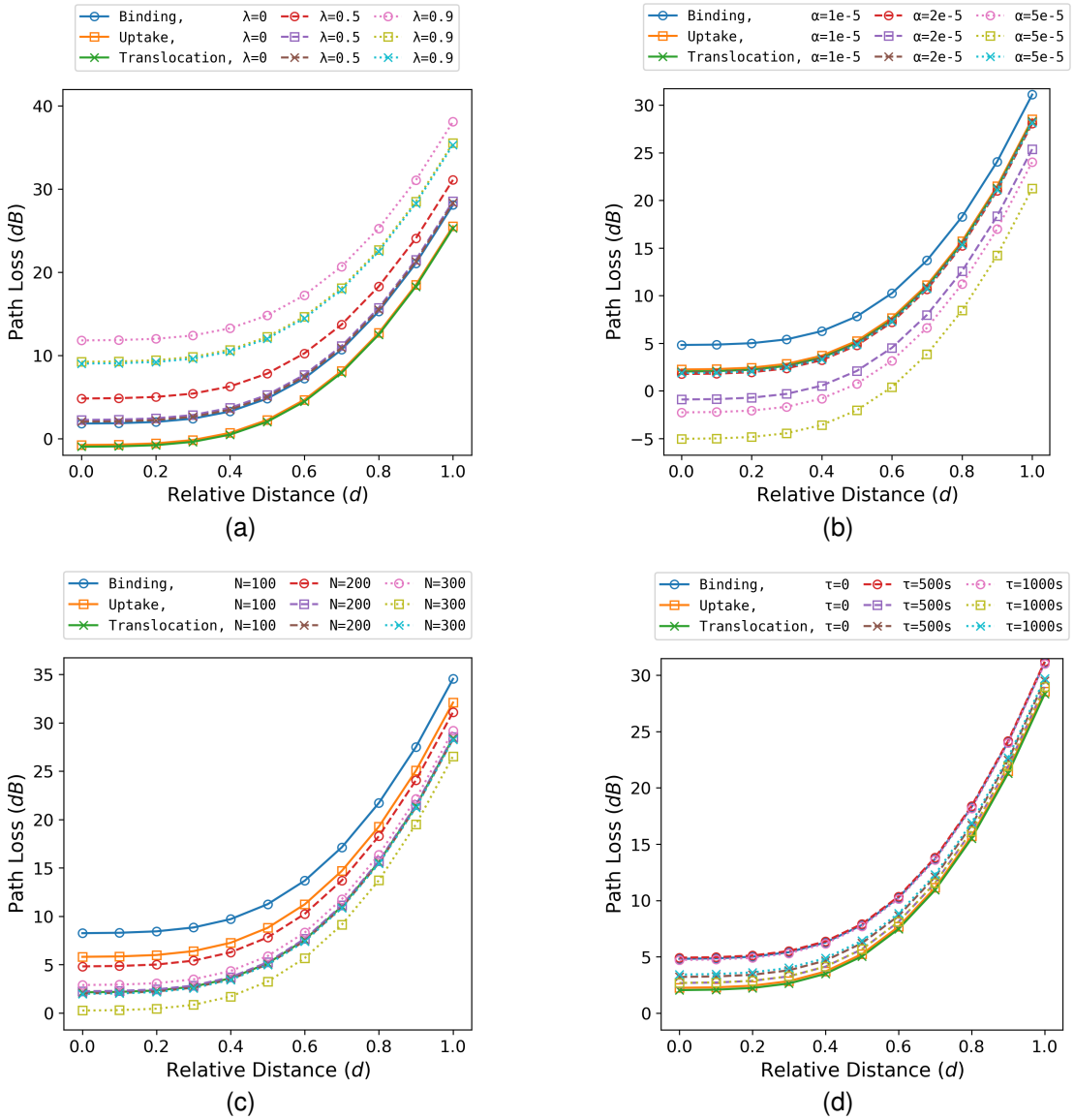

Fig. 3. Path loss profiles of 5'AlaTGC between MC modules. 5'AlaTGC loss under low, mid, and high values for (a) normalised channel tortuosity λ, (b) surface binding rate α, (c) surface capacity constant N, and (d) time delay τ versus the relative source-to-destination distance d.

τ. Taking 5'AlaTGC as our tRF of interest, we observed from Fig. 3a that increasing the tortuosity also increases the molecular processing-induced losses corresponding to the binding, uptake, and translocation processes. This validates the expected reduction in delivered molecules across MC modules when traveling through less permeable media. Next, Figures 3b and 3c illustrates the effect of improving the molecular binding capability of the membrane on the MC modules. We observed that higher membrane binding rates and capacity constants yield lesser molecular processing-induced losses across MC modules. This also proves that the molecular dynamics with faster molecular binding and greater membrane capacity allows for an enhanced molecular uptake, thus also reducing the transmission losses in the succeeding MC modules. We then also explore the effect of introducing an activation delay on the molecular processing-induced losses as the molecules are delivered across MC modules. Interestingly, Fig. 3d shows that time delays produce no significant difference on the binding loss. However, slight increases in uptake and translocation losses were observed for longer time delays which means that activation delays can deteriorate molecular internalization and nuclear translocation. Finally, it can be observed that all three molecular processing-induced losses increase across the above four setups. This confirms the general concept that molecular transmissibility becomes less efficient as the traveling distance of molecules along a medium is lengthened.

C. Communications Performance Analysis

We then evaluate the communications performance of our MC model with respect to the root mean squared error (RMSE)

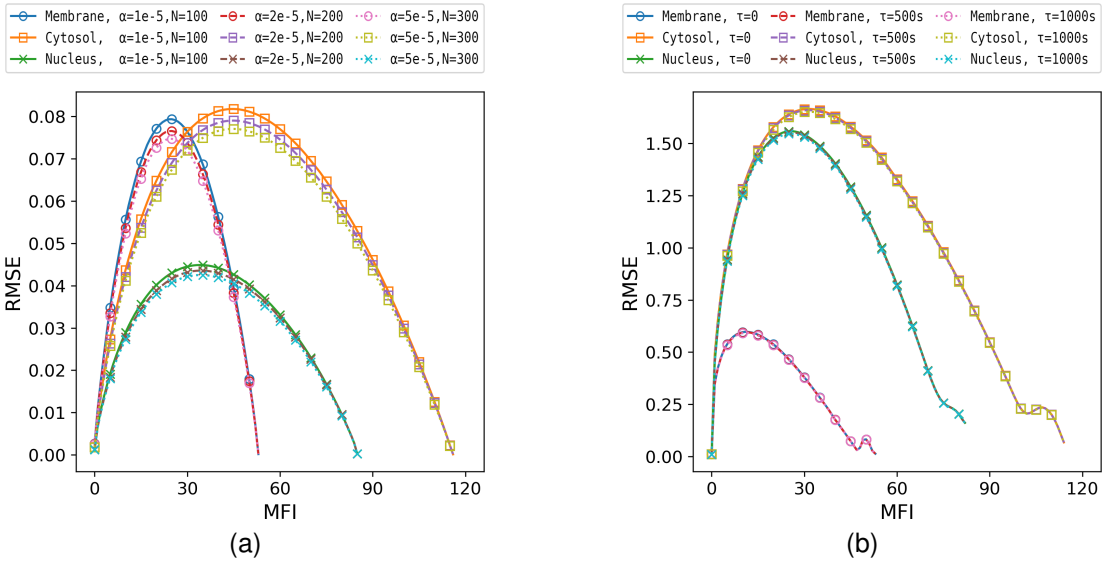

Fig. 4. RMSE of tRF concentrations in the neuron compartments under (a) various surface binding rate α and surface capacity constant N, and (b) time delay τ versus MFI.

versus MFI. We first solve the system in (1) to (4) using Monte Carlo simulations implemented in Python on 1000 randomly sampled channels for each time point t [25]. In Section III-B, we chose low, mid, and high values for the surface binding rate α, surface capacity constant N, and time delay τ to determine the channel variations which follows a normal Gaussian distribution such that $\alpha, N, \tau \sim \mathcal{N}(\mu, \sigma^2)$ where μ was set to each of the low, mid, and high parameter values, and $\sigma = c \cdot \mu$ denotes the standard deviation, with $c = 0.1$ set as the spread factor. We then sum the MFI levels for all three tRFs to represent the total number of transmitted molecules from one MC module to the next. This operation was performed on both true and predicted MC model evaluations for the computation of the RMSE.

The simulations in Fig. 4a have reported higher errors (for $\mathrm{RMSE} \geq 0.03$) for intracellular MC modules, which denotes the total amount of successfully transmitted molecules in the membrane ($\sim 5 < \sum [\mathrm{tRF}]_b <\sim 50$), the cytosol ($\sim 10 < \sum [\mathrm{tRF}]_c <\sim 100$), and the nucleus ($\sim 15 < \sum [\mathrm{tRF}]_n <\sim 65$), for $[\mathrm{tRF}] \in \{[5'\mathrm{AlaTGC}], [5'\mathrm{GluCTC}], [5'\mathrm{GlyGCC}]\}$. These observations correspond to the logistic growth of MFI levels before their stabilisation towards their upper limits. These results verify that the upstream membrane and cytosol have more pronounced variabilities than the downstream nucleus, all of which affect the model output. Moreover, the errors for all intracellular MC modules are slightly reduced when surface binding rate α and capacity constant N are both increased. These also verify that improved molecular binding capabilities leads to a positive impact on the intracellular communications performance.

Next, the simulations in Fig. 4b show that there are no significant error differences for the intracellular MC modules between low, mid, and high time delay τ values, suggesting the independence of MC model variations from activation delays. However, higher errors (for $\mathrm{RMSE} \geq 0.5$) can generally be observed for the total amount of successfully transmitted molecules for both in the cytosol ($\sim 5 < \sum [\mathrm{tRF}]_c <\sim 95$) and the nucleus ($\sim 5 < \sum [\mathrm{tRF}]_n <\sim 70$), in comparison to those bound to the membrane ($\sim 10 < \sum [\mathrm{tRF}]_b <\sim 20$), for $[\mathrm{tRF}] \in \{[5'\mathrm{AlaTGC}], [5'\mathrm{GluCTC}], [5'\mathrm{GlyGCC}]\}$, when activation delays are incorporated in the MC model. Small fluctuations in RMSEs for the intracellular MC modules were also observed as each of their total MFI levels proceed towards their stable upper limits. These results indicate that increasing the time duration for the activation delay does not significantly affect the signal attenuation and molecular throughput of our MC model. However, expressing the proposed delivery system as a delay model demonstrates more variabilities for the downstream cytosol and nucleus MC modules, verifying their dependence on the upstream membrane MC module.

IV. Conclusion

In this paper, we developed an MC model to represent paracrine 5'tRF signalling and therapeutic 5'tRF delivery in neurons by the abstraction of the neuronal microdomain components into MC modules. By characterising tRF expression dynamics as an information throughout model, we have analysed the molecular processing-induced loss and assessed the model communications performance.

The tRF delivery model was structured into the extra- and intra-cellular space of the neuron represented as the molecular channel and molecular receiver, respectively. Further partitions of the molecular receiver include the membrane, cytosol, and nucleus compartments as the receptor, demodulator, and destination, respectively. Interesting findings were made on the effect of enhanced molecular binding capability on the overall model outcome and communications performance. Molecular channel distance and tortuosity also proved to affect

the molecular processing-induced losses, whereas integrating activation time delays to the system can deteriorate molecular internalization and nuclear translocation. The model communications performance was also examined through error analysis to verify the information throughput and path loss results.

While there are limitations on ignoring spatial diffusion and distribution homogeneity for the purposes of this study, our MC model nevertheless describes the paracrine effects of tRFs and may allow for an improvement of their neuroprotective effects in the context of seizure suppression in epilepsy. Based on our results, further simulations and theoretical developments will be beneficial to introduce prediction and treatment strategies for seizure control using the MC approach. This includes modeling the molecular transmitter component of the MC model represented by another neuronal cell secreting the signalling molecules into the molecular channel for their uptake into the molecular receiver. Another approach that uses machine learning to develop the MC model, also called as molecular ML, could be explored with the ultimate aim of developing an improved end-to-end communication system.

ACKNOWLEDGMENTS

K. J. A. P., D. P. M., and D. K. thanks the European Union's EU-FET Open H202 PRIME Project under Grant Agreement No. 964712 for funding this study. S. F., R. S., and J. H. M. P. thanks the Science Foundation Ireland (SFI) under Grant Numbers 16/RC/3948 and 21/RC/10294_P2 for funding this study, as well as the European Regional Development Fund and FutureNeuro industry partners.

REFERENCES

[1] D. C. Henshall, "Microrna and epilepsy: profiling, functions and potential clinical applications," *Curr. Opin. Neurol.*, vol. 27, no. 2, pp. 199–205, Apr. 2014.

[2] K. Tóth *et al.*, "Hyperexcitability of the network contributes to synchronization processes in the human epileptic neocortex," *J. Physiol.*, vol. 596, no. 2, pp. 317–342, Jan. 2018.

[3] L. Kuhlmann, K. Lehnertz, M. P. Richardson, B. Schelter, and H. P. Zaveri, "Seizure prediction - ready for a new era," *Nat. Rev. Neurol.*, vol. 14, no. 10, pp. 618–630, Oct. 2018.

[4] D. C. Henshall *et al.*, "Micrornas in epilepsy: pathophysiology and clinical utility," *Lancet Neurol.*, vol. 15, no. 13, pp. 1368–1376, Dec. 2016.

[5] A. F. Palazzo and E. S. Lee, "Non-coding rna: what is functional and what is junk?" *Front. Genet.*, vol. 6, p. 2, Jan. 2015.

[6] Q. Weng *et al.*, "Extracellular vesicles-associated trna-derived fragments (trfs): biogenesis, biological functions, and their role as potential biomarkers in human diseases," *J. Mol. Med.*, vol. 100, no. 5, pp. 679–695, May 2022.

[7] S. Li, Z. Xu, and J. Sheng, "tRNA-Derived Small RNA: A Novel Regulatory Small Non-Coding RNA," *Genes (Basel)*, vol. 9, no. 52, p. 246, May 2018.

[8] M. C. Hogg *et al.*, "Elevation in plasma trna fragments precede seizures in human epilepsy," *J. Clin. Invest.*, vol. 129, no. 7, pp. 2946–2951, Apr. 2019.

[9] H. McArdle *et al.*, "Quantification of trna fragments by electrochemical direct detection in small volume biofluid samples," *Sci. Rep.*, vol. 10, no. 1, p. 7516, May 2020.

[10] Y. Chahibi, M. Pierobon, S. O. Song, and I. F. Akyildiz, "A molecular communication system model for particulate drug delivery systems," *IEEE Trans. Biomed. Eng.*, vol. 60, no. 12, pp. 3468–3483, Dec. 2013.

[11] Y. Chahibi, M. Pierobon, and I. F. Akyildiz, "Pharmacokinetic modeling and biodistribution estimation through the molecular communication paradigm," *IEEE Trans. Biomed. Eng.*, vol. 62, no. 10, pp. 2410–2420, Oct. 2015.

[12] M. Veletić, M. T. Barros, I. Balasingham, and S. Balasubramaniam, "A molecular communication model of exosome-mediated brain drug delivery," in *2019 ACM NanoCom Conf. Proc.*, no. 22, Sep. 2019, pp. 1–7.

[13] M. Veletić, M. T. Barros, H. Arjmandi, S. Balasubramaniam, and I. Balasingham, "Modeling of modulated exosome release from differentiated induced neural stem cells for targeted drug delivery," *IEEE Trans. Nanobiosci.*, vol. 19, no. 3, pp. 357–367, Jul. 2020.

[14] K. J. McKelvey, K. L. Powell, A. W. Ashton, J. M. Morris, and S. A. McCracken, "Exosomes: Mechanisms of uptake," *J. Circ. Biomark.*, vol. 4, p. 7, Jul. 2015.

[15] E. Sykovà and C. Nicholson, "Diffusion in brain extracellular space," *Physiol. Rev.*, vol. 88, no. 4, pp. 1277–1340, Oct. 2008.

[16] S. Qiu *et al.*, "Molecular channel fading due to diffusivity fluctuations," *IEEE Commun. Lett.*, vol. 21, no. 3, pp. 676–679, Mar. 2017.

[17] T. Nakano, Y. Okaie, and J. Q. Liu, "Channel model and capacity analysis of molecular communication with brownian motion," *IEEE Commun. Lett.*, vol. 16, no. 6, pp. 797–800, Jun. 2012.

[18] J. Hrabe, S. Hrabětová, and K. Segeth, "A model of effective diffusion and tortuosity in the extracellular space of the brain," *Biophys. J.*, vol. 87, no. 3, pp. 1606–1617, Sep. 2004.

[19] H. B. Yilmaz, C. M. Lee, Y. J. Cho, and C. B. Chae, "A machine learning approach to model the received signal in molecular communications," in *2017 IEEE BlackSeaCom Conf. Proc.*, 2017, pp. 1–5.

[20] D. Vimalajeewa and S. Balasubramaniam, "Digestive system dynamics in molecular communication perspectives," in *2021 BICT Conf. Proc.*, 2021, pp. 117–133.

[21] H. Itagaki, "Fluorescence Spectroscopy," in *Experimental Methods in Polymer Science*. T. Tanaka, 2000, ch. 3, pp. 155–260.

[22] D. P. Martins, K. Leetanasaksakul, M. T. Barros, A. Thamchaipenet, W. Donnelly, and S. Balasubramaniam, "Molecular communications pulse-based jamming model for bacterial biofilm suppression," *IEEE Trans. Nanobioscience*, vol. 17, no. 4, pp. 533–542, Oct. 2018.

[23] D. P. Martins, J. Drohan, S. Foley, L. Coffey, and S. Balasubramaniam, "Modulated molecular channel coding scheme for multi-bacterial transmitters," in *2021 ACM SenSys Conf. Proc.*, 2019, pp. 610–615.

[24] P. Ivanov, M. M. Emara, J. Villen, S. P. Gygi, and P. Anderson, "Angiogenin-induced trna fragments inhibit translation initiation," *Mol. Cell*, vol. 43, no. 4, pp. 613–623, Aug. 2011.

[25] S. Abdallah and A. M. Darya, "Semi-blind channel estimation for diffusive molecular communication," *IEEE Commun. Lett.*, vol. 24, no. 11, pp. 2503–2507, Nov. 2020.